Pergamon

Int. J. Heat Mass Transfer. Vol. 38, No. 10, pp. 1865–1878, 1995

0017-9310/95 $9.50+0.00

0017-9310(94)00306-8

Unsteady analysis of non-isothermal flow and heat transfer between rotating co-axial disks

C. Y. SOONG
Department of Aeronautical Engineering, Chung Cheng Institute of Technology, Taoyuan, Taiwan 33509, Republic of China

and

H. L. MA†
Department of System Engineering, Chung Cheng Institute of Technology, Taoyuan, Taiwan 33509, Republic of China

(*Received* 30 *May* 1994 *and in final form* 25 *August* 1994)

Abstract—In the present investigation a theoretical analysis is performed to study the unsteady mixed convection flow and heat transfer between two infinite coaxial isothermal disks. One disk rotated at a constant rate and another one at a time-dependent rate. Two modes of the time-dependent rotation, asymptotic and torsionally oscillatory, are studied. Governing equations are formulated with respect to a rotating frame of reference. The density variation in the centrifugal force term is considered to explore the rotation-induced buoyancy effect. By using proper transformations, a simple model of spatial similarity for a Boussinesq fluid is developed and then solved by a finite-difference method. Effects of rotation, centrifugal buoyancy, unsteadiness, oscillation amplitude and frequency on the flow and heat transfer characteristics are discussed.

INTRODUCTION

Fluid flow and heat transfer associated with a rotating disk system are of academic and practical interest for the wide applications of rotating machinery. Due to the rotation of the disk two rotational forces, Coriolis and centrifugal, are present in the flow field. By considering the fluid density variation and invoking the Boussinesq approximation, the so-called centrifugal buoyancy can be taken into account. The buoyancy effects on steady transport phenomena in rotating disk systems have been extensively studied by Soong and his colleagues [1–3]. In a rotating thermal system, the heat transfer performance may be enhanced or reduced by the transient effects. In the worst cases of heat transfer degradation, damage may result by the periodic and/or excessive thermal loading as well as the emergence of the local hot spot. To explore the unsteady flow characteristics, in the past, the transient analyses associated with rotating disk systems have been studied by a number of investigators. The related flow configurations can be roughly divided into the following three categories: (1) single disk [4–14]; (2) coaxial disks [15, 16] and (3) cylindrical container [17–21]. Additionally, unsteady film flow on a rotating disk, e.g. that in refs. [22, 23], is another kind of rotating-disk flow configuration. The central theme of the latter class of studies lies in the interfacial effects and is quite different from that of the problems in the aforementioned three categories.

A chronological list of the previous theoretical/numerical works on unsteady rotating flows associated with the single disk, coaxial disks, and cylindrical container is shown in Table 1. Some characteristic features of the unsteady rotating-disk flows have been disclosed in the former literature. For example, in an impulsively started rotating-disk system, the time for development of the steady state and Ekman layer is of the order of $Re^{1/2}$ [19]. In Sharma's analysis for a single fluctuating disk [14], it has been revealed that the responses of the heat transfer rate and the radial friction present phase lag, while the tangential friction is phase leading. Later on, Singh's results [14] corroborated Sharma's conclusion; also, he found small effects of frequency on heat transfer rates. From the aforementioned literature survey, most of the studies focused their attention on hydrodynamic natures, and only a few studies [8, 12, 14] have dealt with forced convection heat transfer on a single disk. Moreover, it is noted that only two studies pertain to the unsteady flow in the coaxial disk system. Up to date, strictly speaking, a study on the unsteady non-isothermal flow and heat transfer characteristics between two rotating disks has not yet been reported.

The objective of the present work is to study the effects of the transient rotation and the centrifugal

† Present address: Assistant Scientist, Propulsion Group, Aeronautical Industrial Development Center, Taichung, Taiwan 400, Republic of China.

NOMENCLATURE

B buoyancy parameter or thermal Rossby number, $\beta\Delta T_c$
C_f skin friction coefficient, $2\mu(\partial U/\partial Z)_w/[\rho(R\Omega_1)^2]$
c_p constant-pressure specific heat
F radial velocity function, $U/R\Omega_1$
G tangential velocity function, $V/R\Omega_1$
H axial velocity function, $W/(\nu\Omega_1)^{1/2}$
h heat transfer coefficient
k thermal conductivity
Nu Nusselt number, hS/k
P static pressure
P', p' dimensionless and dimensional pressure departure, $P' = p'/\rho(S\Omega_1)^2$
Pr Prandtl number, ν/α
R, φ, Z cylindrical coordinates
Re^* local rotational Reynolds number, $(R\Omega_1)S/\nu$
Re rotational Reynolds number, $\Omega_1 S^2/\nu$
S spacing between two coaxial disks
T temperature
t time
ΔT_c characteristic temperature difference, $T_2 - T_1$
U, V, W velocity components in R–φ–Z coordinate system.

Greek symbols

α thermal diffusivity, $k/\rho c_p$
β thermal expansion coefficient, $-(1/\rho_r)(\partial\rho/\partial T)_r$
γ dimensionless disk-velocity difference, $(\Omega_2 - \Omega_1)/\Omega_1$
η dimensionless axial coordinate, Z/S
θ dimensionless temperature difference, $(T - T_1)/\Delta T_c$
μ dynamic viscosity
ν kinematic viscosity, μ/ρ
Π dimensionless pressure, $P'/\rho_r(S\Omega_1)^2$
ρ density
τ dimensionless time, $\Omega_1 t$
Ω rotational speed (rsd s^{-1} or rpm)
ω, Ω_{OS} dimensionless and dimensional forcing frequency, $\omega = \Omega_{OS}/\Omega_1$.

Subscripts

0 initial state
1 first disk
2 second disk
∞ asymptotic state as $t \to \infty$
r reference or radial
t tangential
Ω rotation.

buoyancy on flow and heat transfer between two coaxially rotating infinite isothermal disks. One of the disks rotates at a constant rate and another one at a time-dependent rotating rate. The density variation in the centrifugal force term is considered so as to account for the centrifugal-buoyancy effects. The governing equations for the Boussinesq fluid with respect to a rotating frame of reference are trans-

Table 1. Previous theoretical/numerical studies on unsteady rotating disk flow and heat transfer problems

Author	Year	Rotating system	Solution	Heat convection	Unsteady mode
Rosenbalt	1959	Single disk	Asymptotic	—	Oscillatory
Rosenbalt	1960	Coaxial disks	Asymptotic	—	Oscillatory
Greenspan and Howard	1963	Cylindrical container	Asymptotic	—	Impulsive
Benney	1963	Single disk	Asymptotic	—	Oscillatory
Wedemeyer	1964	Cylindrical container	Integral	—	Impulsive
Riley	1965	Single disk	Asymptotic	—	Oscillatory
Pearson	1965	Coaxial disks	Finite difference	—	Impulsive
Benton	1966	Single disk	Series	—	Impulsive
Riley	1967	Single disk	Asymptotic	Forced	Impulsive Oscillatory
Pao	1970	Cylindrical container	Finite difference	—	Impulsive
Lugt and Haussling	1973	Cylindrical container	Finite difference	—	Impulsive
Bodonyi and Stewartson	1977	Single disk	Finite difference	—	Impulsive
Purushothaman	1978	Single disk	Asymptotic	—	Oscillatory
Shippers	1978	Single disk	Finite difference Asymptotic	—	Impulsive Oscillatory
Sharma	1979	Single disk	Asymptotic	Forced	Oscillatory
Bertela and Gori	1982	Cylindrical container	Finite difference	—	Impulsive
Stewartson *et al.*	1982	Single disk	Asymptotic	—	Impulsive
Singh *et al.*	1989	Single disk	Finite difference	Forced	Oscillatory

formed to a spatial similarity form. A number of previous investigations, see Table 1, used asymptotic expansion in their analyses; however, the results were restricted to the extreme cases of low- and high-frequency flows. In the present work, a finite difference method is used for solution of the unsteady spatial-similarity equations. Although, as disclosed in a recent review article by Mochizuki [24], the rotating disk flows are complex because of flow turbulence and rotating stall phenomenon for high rotation rate and large radius, the similarity analysis is still useful for exploration of the laminar and stall-free part of the flow field. For example, in the comparisons made by Pearson [16] and Itoh *et al.* [25], similarity solutions seem in reasonable agreement with the finite-disk data in the region of $R/S \leqslant 0.6$. This lends supports for the usefulness of the similarity models. The same class of models has been employed to study various unsteady flows, e.g. rotating-disk flow (without heat transfer) [16] and the film flow on a rotating disk [23]. Moreover, since the measurements of the field properties, e.g. velocities and temperature, on the two-disk flow configurations are quite difficult, especially for the temperature distributions in the torsionally oscillating flow considered, a relatively simple theoretical model can provide some useful qualitative and/or quantitative results, and play a complementary role in understanding hydrodynamic and heat transfer characteristics of this class of complex flows. In the present work, two modes of unsteady rotation, asymptotic and torsionally oscillatory, are considered. The influences of the rotation, centrifugal buoyancy and unsteadiness, including the effects of frequency and amplitude, on the flow and heat transfer characteristics are discussed.

ANALYSIS

As shown in Fig. 1, two rotating coaxial infinite disks considered in the present study are placed in parallel and separated by a spacing S. The disks lie at constant wall temperatures T_1 and T_2, and rotate at rotational speeds Ω_1 and Ω_2, respectively. The rotational rate Ω_1 is constant and that of disk 2 is time dependent, i.e. $\Omega_2 = \Omega_2(t)$. The cylindrical coordinate system is fixed on the center of the disk 1 and rotates with it. Assume that the flow is laminar, axisymmetric, and of constant physical properties. By invoking the Boussinesq approximation to allow for density variation in centrifugal force term, the governing equations can be written in a similar form as appeared in a previous steady work [26]:

$$\nabla \cdot \mathbf{V} = 0 \tag{1}$$

$$\partial \mathbf{V}/\partial t + (\mathbf{V}\cdot\nabla)\mathbf{V} = \nu\nabla^2\mathbf{V} + \nabla P'/\rho_r - \beta(T-T_r)(\Omega\times\Omega\times\mathbf{R}) - 2\Omega\times\mathbf{V} \tag{2}$$

$$\partial T/\partial t + (\mathbf{V}\cdot\nabla)T = \alpha\nabla^2 T \tag{3}$$

where the subscript r denotes a reference condition at which $\mathbf{V} \equiv 0$, $P' = P - P_r$ is the pressure departure from the reference condition, and $\mathbf{R}$ is the position vector. By using the transformations and the dimensionless parameters:

$$\eta = Z/S, \quad \tau = \Omega_1 t, \quad F = U/R\Omega_1, \quad G = V/R\Omega_1,$$

$$H = W/(\nu\Omega_1)^{1/2}, \quad \theta = (T-T_1)/\Delta T_c, \quad Re = S^2\Omega_1/\nu,$$

$$Pr = \nu/\alpha, B = \beta\Delta T_c, \Delta T_c = T_2 - T_1$$

the governing equations can be written as

$$G_\tau = Re^{-1}G_{\eta\eta} - Re^{-1/2}(HG_\eta - H_\eta G - H_\eta) \tag{4}$$

$$H_{\tau\eta\eta} = Re^{-1}H_{\eta\eta\eta\eta} - 4Re^{1/2}(G+1)G_\eta - Re^{-1/2}HH_{\eta\eta\eta} + 2BRe^{1/2}\theta_\eta \tag{5}$$

$$\theta_\tau = (Pr\,Re)^{-1}\theta_{\eta\eta} - Re^{-1/2}H\theta_\eta \tag{6}$$

with the boundary and initial conditions for $H(\tau,\eta)$, $G(\tau,H)$ and $\theta(\tau,\eta)$ given as follows:

$$H(\tau,0) = H'(\tau,0) = H(\tau,1) = H'(\tau,1) = 0$$

$$G(\tau,0) = G(\tau,1) - \gamma(\tau) = 0$$

$$H(0,\eta) = H_0(\eta), G(0,\eta) = G_0(\eta), \theta(0,\eta) = \theta_0(\eta) \tag{7}$$

where $G(\tau,\eta)$, $H(\tau,\eta)$ and $\theta(\tau,\eta)$ are the tangential velocity, axial velocity and temperature function, respectively. Note that the radial velocity $F(\tau,\eta)$ has been expressed in terms of the derivative $H_\eta(\tau,\eta)$.

The parameter Pr is the Prandtl number and $Pr = 0.7$ for air is used in the present study. The rotational effect is characterized by the Reynolds number, Re, which ranges from 10 to 1200. The buoy-

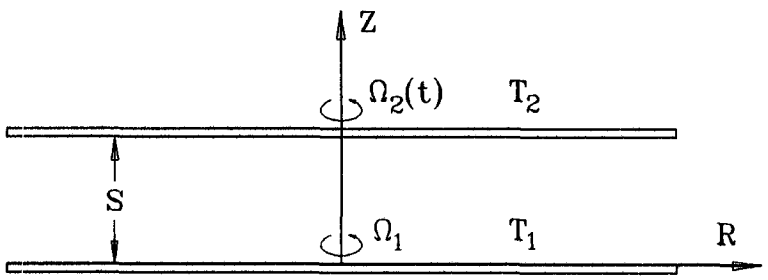

Fig. 1. Physical model of rotating coaxial disks.

Table 2. Grid-dependence of the friction factors and Nusselt numbers for (Re, B, γ_0, γ_∞, σ, $\Delta\tau$) = (100, 0.2, −1, 0, 0.8, 2.5×10^{-4})

No. of grids	51	101	201
$C_{fr1}\,Re^*$	−3.10502 (0.773%)	−3.09026	−3.09026
$C_{fr2}\,Re^*$	+0.238285 (0.928%)	+0.238473	+0.238473
$C_{ft1}\,Re^*$	−11.2301 (0.458%)	−11.2714	−11.2714
$C_{ft2}\,Re^*$	−3.86619 (3.000%)	−3.94722	−3.94722
Nu_1	+10.3034 (0.595%)	+10.3675	+10.3675
Nu_2	+2.25832 (0.010%)	+2.27522	+2.27522

ancy parameter B is also referred to as the thermal Rossby number. For validity of the Boussinesq approximation, in conventional free-convection problems, the values of $B = \beta\Delta T_c$ were usually small. For example, a magnitude of $\beta\Delta T_c \leqslant 0.1$ was claimed in the study of Gray and Giorgini [27]; and a value of 0.2 was also used [28]. In the present work, the thermal Rossby number B is restricted in the range of $|B| \leqslant 0.2$, and $\gamma(\tau) \equiv [\Omega_2(\tau)-\Omega_1]/\Omega_1$ is the dimensionless rotation-rate difference between the two disks. The values of $\gamma = 0$, -1 and -2, respectively, correspond to the cases of $\Omega_2 = \Omega_1$ (co-rotating disks), $\Omega_1 \neq \Omega_2 = 0$ (rotor-stator) and $\Omega_2 = -\Omega_1$ (counter-rotating disks). The radial velocity $F(\tau, \eta)$ can be evaluated by continuity once $H(\tau, \eta)$ has been solved. The functions $H_0(\eta)$, $G_0(\eta)$ and $\theta_0(\eta)$ stand for the steady-state solutions corresponding to the initial rotational condition $\gamma_0 = \gamma(0)$. In the present study both the asymptotically varying rotation rate $\gamma(\tau)$

$$\gamma(\tau) = \gamma_0 + (\gamma_\infty - \gamma_0)(1-\sigma^\tau) \quad 0 < \sigma < 1 \tag{8}$$

and the torsionally oscillatory mode

$$\gamma(\tau) = \gamma_0 + \zeta \sin(\omega\tau) \tag{9}$$

are considered. In equation (8), $\gamma_\infty = \gamma(\infty)$ denotes the asymptotic state as $\tau \to \infty$; the parameter σ is one governing the rate of change of γ, ζ in equation (9) stands for the oscillation amplitude, and $\omega = \Omega_{OS}/\Omega_1$

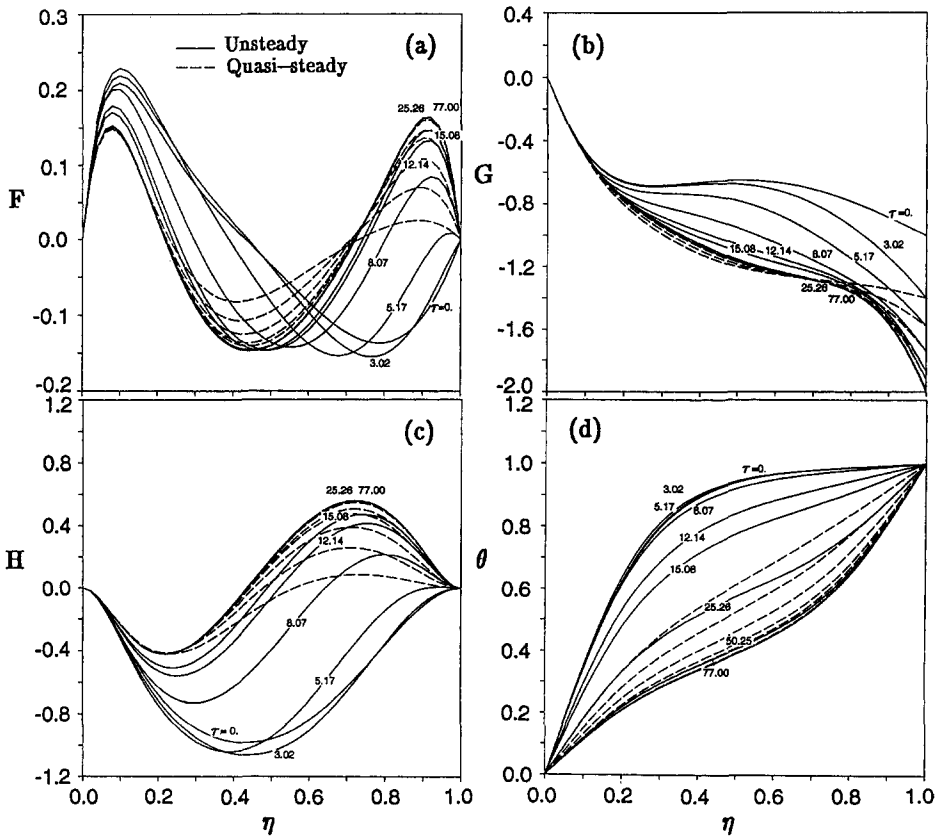

Fig. 2. Spin-up solutions for (Re, B, γ_0, γ_∞, σ) = (100, 0.1, −1, −2, 0.845).

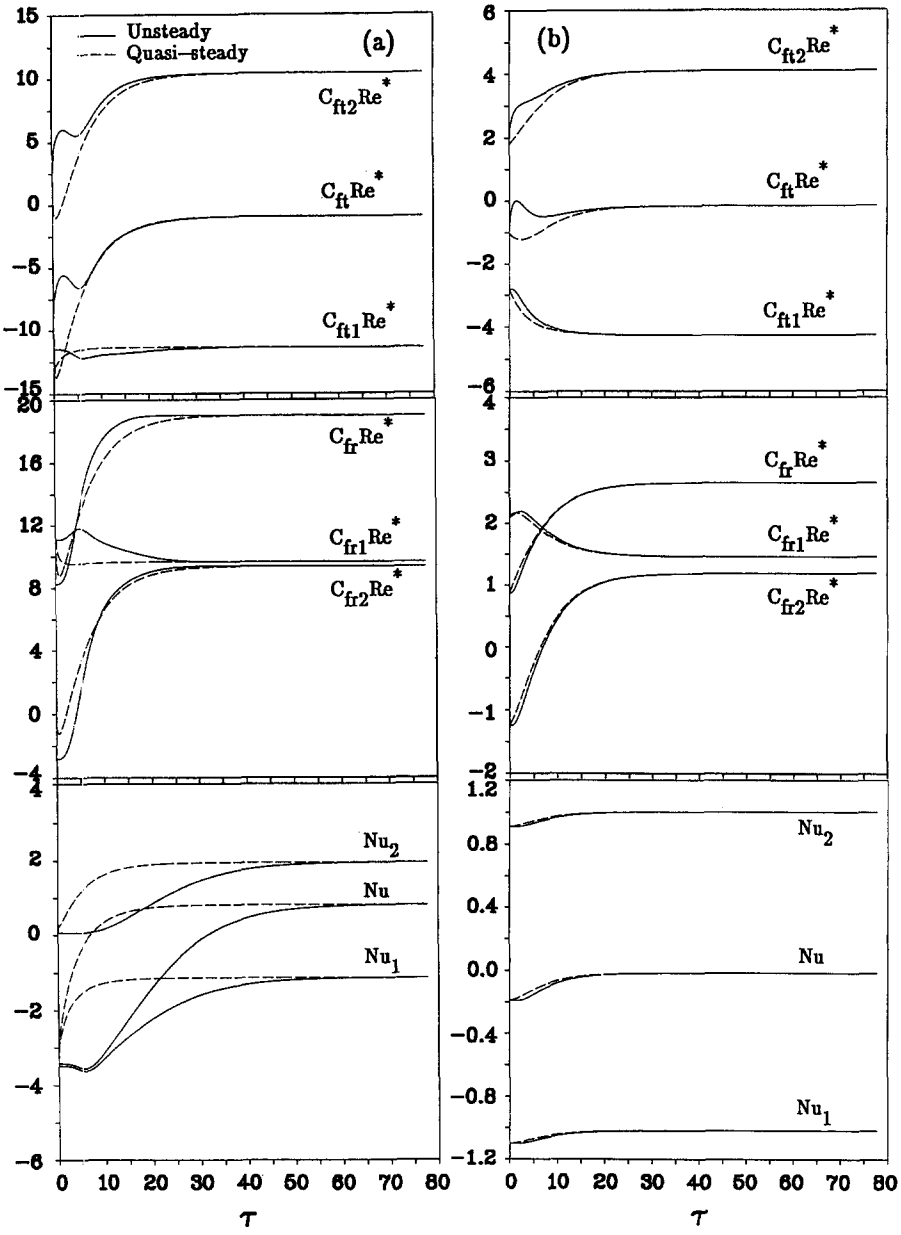

Fig. 3. Friction factors and heat transfer rates for $(B, \gamma_0, \gamma_\infty, \sigma) = (0.1, -1, -2, 0.845)$. (a) $Re = 100$, (b) $Re = 10$.

and Ω_{OS} are the dimensionless and dimensional frequency of the disk oscillation.

The flow and heat transfer parameters concerned in the present study are tangential and radial skin friction and heat transfer rate. These boundary parameters on each disk and the two-disk summations are defined as follows.

(a) Tangential skin friction factors:

$$C_{ft1}\,Re^* = 2G_\eta(\tau,0) \quad C_{ft2}\,Re^* = -2G_\eta(\tau,1)$$
$$C_{ft}\,Re^* = C_{ft1}Re^* + C_{ft2}\,Re^* \tag{10}$$

(b) Radial skin friction factors:

$$C_{fr1}\,Re^* = 2F_\eta(\tau,0) \quad C_{fr2}\,Re^* = -2F_\eta(\tau,1)$$
$$C_{fr}\,Re^* = C_{fr1}\,Re^* + C_{fr2}\,Re^* \tag{11}$$

(c) Nusselt numbers:

$$Nu_1 = -\theta_\eta(\tau,0) \quad Nu_2 = \theta_\eta(\tau,1)$$
$$Nu = Nu_1 + Nu_2. \tag{12}$$

By these definitions, the positive values of the Nusselt number stand for the heat transferred from

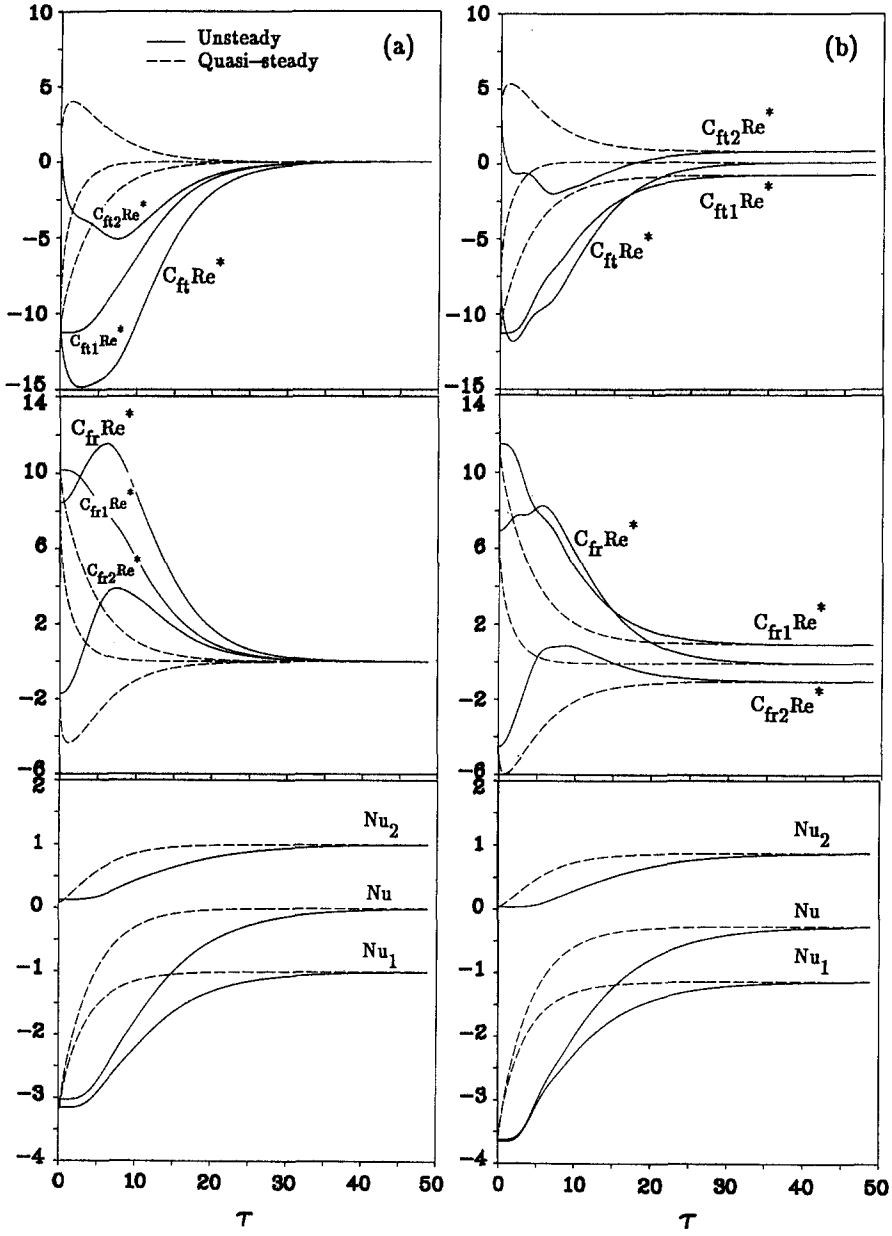

Fig. 4. Buoyancy effects on friction factors and heat transfer rates for $(Re, \gamma_0, \gamma_\infty, \sigma) = (100, -1, 0, 0.8)$. (a) $B = 0.0$ and (b) $B = 0.2$.

the wall to fluid, and the negative Nu for heat transfer from wall to fluid in the case of $T_2 - T_1$. The situation is reversed for $T_1 > T_2$.

NUMERICAL PROCEDURE

The numerical computation is carried out on a nonuniform algebraic grid. Time-wise discretization is carried out by using a weighted scheme [29], while the spatial discretization is performed by a three-point exponential-based scheme, which was originally developed by Barrett [30] and recently extended to a nonuniform-discretization form by Soong [31].

Numerical experiments on the grid-dependence test were performed. A typical case of a rotor-stator system ($\gamma = -1$) at $Re = 100$, $B = 0.2$ and $Pr = 0.7$ was considered as an illustrative example. Disk 2 was initially stationary and impulsively started at $\tau = 0$, and then approached $\Omega_2 = \Omega_1$. In this situation, $\gamma(\tau)$ varied from $\gamma_0 = -1$ to $\gamma_\infty = 0$ with $\sigma = 0.8$. A uniform time step, $\Delta\tau = 2.5 \times 10^{-4}$, is used in the test. Table 2 lists the results at $\tau = 5.0$ (20 000th time step) on grids of 51, 101, 201 points in η-space. Solutions on the 101-grid show no significant deviation from the 201-grid results. The deviations of the 51-grid solutions from the 201-grid ones are shown in the par-

entheses. It is obvious that, in this case, the 101-grid is sufficient for accuracy. For high-Re cases ($Re \geqslant 500$) a finer grid, e.g. 201-point, has to be used for better resolution and convergence characteristics. The effect of the time step was also studied: for $\sigma = 0.8$ and 0.845 considered in the present work, the results revealed that $\Delta\tau$ of order 10^{-4} is appropriate in the computation. However, for the smaller σ in the asymptotic mode, i.e. rapid time rate of change in γ, a smaller time step should be employed.

RESULTS AND DISCUSSION

Asymptotic mode

Transient effects and formation of Ekman layer. Figure 2 shows the results for the case of $Re = 100$, $B = 0.1$. Disk 2 is initially stationary, $\Omega_2 = 0$, and then suddenly spins up in the opposite direction to disk 1, and then approaches to $\Omega_2 = -\Omega_1$ asymptotically. Therefore, the value of γ changes from $\gamma_0 = -1$ to $\gamma_\infty = -2$ following the rule of equation (8) with $\sigma = 0.845$. In Fig. 2(a), the evolution of radial velocity demonstrates the formation of the Ekman layer at $\eta = 1.0$ due to spin up of disk 2. All the velocity components in Figs. 2(b)–(d) evolve fast at the transient stage, $\tau < 25$: beyond that value the system approaches a steady state asymptotically. The differences between the velocity solutions at $\tau = 25.26$ and 77.00 are insignificant. However, the temperature field is not so sensitive to the disturbance. Even at $\tau = 50.25$, θ still does not reach its steady state. The responses of friction factors and Nusselt numbers in Fig. 3(a) can also demonstrate this phenomenon. At $\tau = 77.00$, the solutions, including flow and temperature fields, coincide (almost) with the steady state of $Re = 100$, $B = 0.1$ and $\gamma = -2$.

Reynolds number effects. Figures 3(a) and (b), respectively, present the skin friction and heat transfer rate for the cases of $Re = 100$ and $Re = 10$; and both cases are of $B = 0.1$, $\gamma_0 = -1$, $\gamma_\infty = -2$ and $\sigma = 0.845$. Like in an impulsively started system the responses of the flow and temperature fields cannot follow the variation in time. By comparing Figs. 3(a) and (b), it is noted that the transient effects, which are characterized by the deviations of the unsteady solutions and the quasi-steady ones solved by considering the temporal value of $\gamma(\tau)$ as a constant, are more remarkable for the higher Reynolds number, $Re = 100$. The larger transient effects in this situation can be attributed to the relatively stronger inertia in rapidly rotating systems. Comparison of the unsteady solutions with the quasi-steady ones of the heat transfer rates reveals that the transient effect diminishes at time about $\tau = 70$ for $Re = 100$, while at about $\tau = 20$ for $Re = 10$.

Buoyancy effects. For the case of $Re = 100$, disk 2 is impulsively started at $\tau = 0$ and, then, the rotation rate $\Omega_2(\tau)$ approaches to Ω_1 asymptotically with $\sigma = 0.8$. Equivalently, $\gamma(\tau)$ varies from $\gamma_0 = -1$ to $\gamma_\infty = 0$. In this situation, the time evolutions of the radial friction factors and heat transfer rates with buoyancy parameter $B = 0.0$ and 0.2 are respectively shown in Figs. 4(a) and (b), wherein the unsteady solutions are compared with the quasi-steady solutions. In the comparison, the buoyancy effects influence the solutions only quantitatively. Since the final state is of $\gamma = 0$, i.e. two disks rotating at the same rate, the friction factors on the disks all settle down to the zero level for the solid-rotation case, i.e. $\gamma = B = 0.0$ in Fig. 4(a), and Nusselt numbers correspond to a conduction solution as expected. For $B = 0.2$ in Fig. 4(b), it is a free-convection flow driven

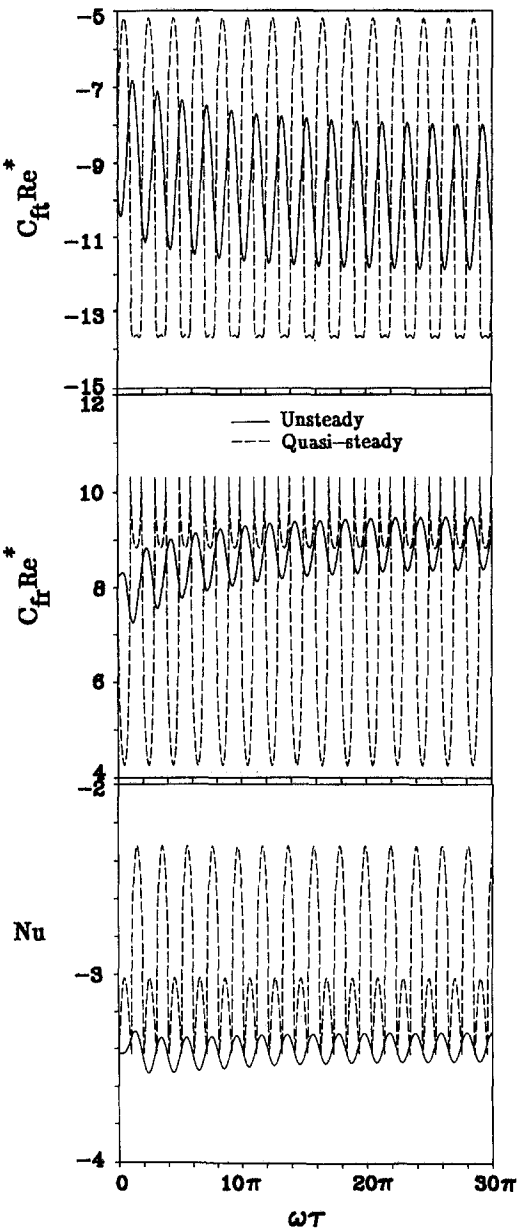

Fig. 5. Transient development of flow and heat transfer parameters for (Re, B, γ_0, ζ, ω) = (100, 0.1, −1, 0.1, 0.2π)

by the centrifugal buoyancy [2]. From the results in Figs. 4(a) and (b), the responses in the two cases are quite similar. It means that the development of the transient stage is not significantly altered by the centrifugal buoyancy effect in the transient flows of asymptotic mode.

Oscillatory mode

Transient stage and fully developed oscillation. Figure 5 shows the flow and heat transfer parameters for the combination of the governing parameters: (Re, B, γ_0, ζ, ω) = (100, 0.1, -1, 0.1, 0.2π). The system reaches a fully developed periodicity after 12 cycles, i.e. $\omega\tau = 24\pi$: before that the system lies at a transient stage with a variable mean. Herein the term 'fully-developed periodicity' means the system repeats itself cyclically. In Fig. 5, the fully-developed oscillation is of a time-invariant mean, amplitude and frequency. By comparing with the quasi-steady results the variations of the skin friction and heat transfer rate are alleviated in the presence of unsteadiness.

Reynolds number effects. The Reynolds number

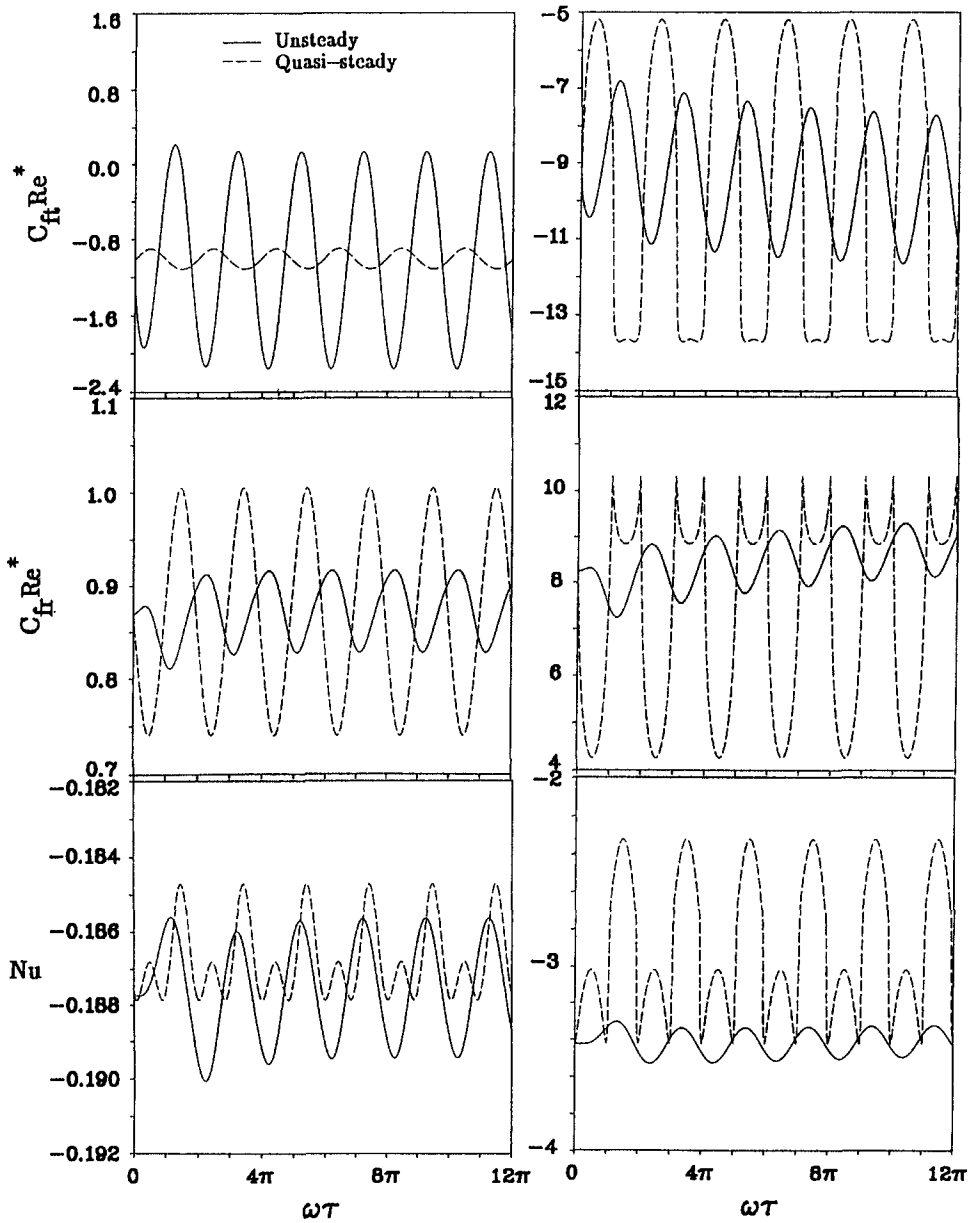

Fig. 6. Reynolds number effects on the oscillatory behaviors for flow at (B, γ_0, ζ, ω) = (0.1, -1, 0.1, π). (a) Re = 10 and (b) Re = 100.

effects on the oscillatory behaviors are shown in Fig. 6, wherein the friction factors and Nusselt numbers for $Re = 10$ and 100 under the conditions $(B, \gamma_0, \zeta, \omega) = (0.1, -1, 0.1, \pi)$ are plotted. In the flow at $Re = 10$, as shown in Fig. 6(a), the transient stage sustains about three cycles, i.e. $\omega\tau = 6\pi$; while for the relatively higher Reynolds number, i.e. $Re = 100$ in Fig. 6(b), a longer period is needed for the transient development. It is noticed that, due to the inertia, the temporal responses in the unsteady flows generally deviate from their quasi-steady counterparts remarkably. For the torsional oscillation of disk 2, the tangential friction of disk 2, $C_{ft2}\,Re^*$, can be augmented by the transient effect. In Fig. 6(b), the unsteady results of $C_{ft2}\,Re^*$ for the relatively higher Reynolds number, $Re = 100$, are alleviated. Also, in Fig. 6(b), the responses reveal that the differences between the temporal responses and the corresponding quasi-steady flows are more pronounced in a high Reynolds number flow for the strong inertia.

Figure 7(a) shows the cyclic evolution of the tangential velocity in an oscillatory period for a typical

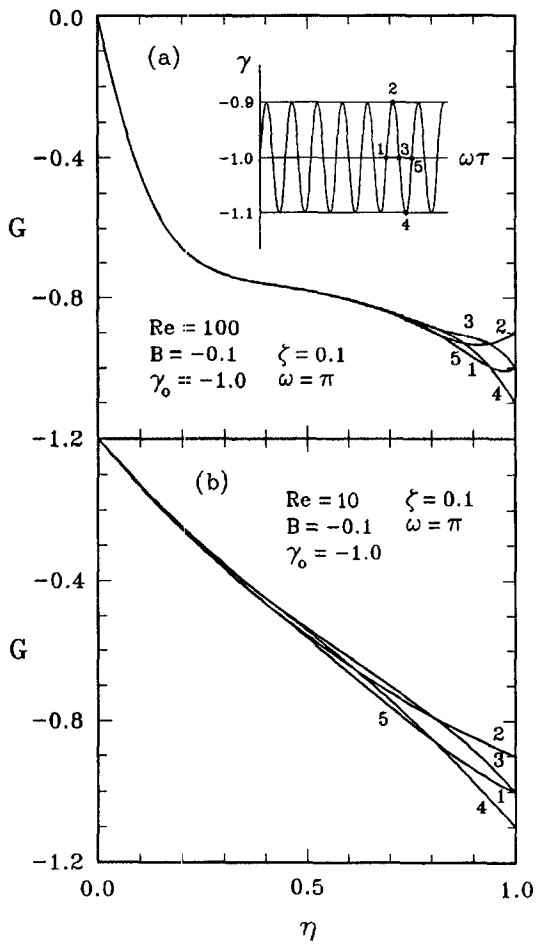

Fig. 7. Cyclic evolution of tangential flow at $(B, \gamma_0, \zeta, \omega) = (-0.1, -1, 0.1, \pi)$. (a) $Re = 100$, (b) $Re = 10$.

case of $(Re, B, \gamma_0, \zeta, \omega) = (100, -0.1, -1, 0.1, \pi)$ in fully-developed oscillation regime, in which the response of the tangential velocity is the most salient one among three velocity components and the temperature field. The time-evolution of the tangential motion near the oscillatory disk can be observed clearly, while the temporal change in the region of $\eta < 0.7$ is insignificant. For a relatively low Reynolds number, $Re = 10$ in Fig. 7(b), the penetration depth or influenced region of the disk oscillation can be extended due to the small inertia of the flow system.

Buoyancy effects. For the case of $(Re, \gamma_0, \zeta, \omega) = (100, -1, 0.1, 0.2\pi)$, the total tangential and radial friction factors and Nusselt numbers with buoyancy parameters $B = 0.2$, 0 and -0.2 are presented in Fig. 8. By examining the transient development process, it can be found that the responses for $B = 0.2$ present a longer transient stage than the cases of $B = 0$ and -0.2.

In the plots of tangential factors, $C_{ft1}\,Re^*$ and $C_{ft2}\,Re^*$, it is revealed that $C_{ft2}\,Re^*$ in this case stays very close to the quasi-steady solution, and the magnitudes of the amplitudes for $B = -0.2$ and 0.2 both do not change too much as compared with that for $B = 0$. The amplitude of $C_{ft1}\,Re^*$ for $B = 0$ is about 20% of the quasi-steady solution. Comparatively, the amplitude of the $C_{ft1}\,Re^*$ response is large for $B = 0.2$ (>0) and small for $B = -0.2$ (<0). In other words, centrifugal buoyancy with $T_2 > T_1$ enhances the transient effect and the buoyancy effect with $T_1 > T_2$ $[B = -0.2\ (<0)]$ reduces the transient effect. The same phenomena can also be observed in the plots of the boundary parameters $C_{fr1}\,Re^*$, $C_{fr2}\,Re^*$ and Nu_1. On the contrary, the influence of the buoyancy is reversed in the behavior of the heat transfer on disk 2, Nu_2. The centrifugal buoyancy with positive B reduces the amplitude of the Nu_2 response, while that with negative B enhances it. The centrifugal-buoyancy effect also shifts the phase of the responses. For example, in the tangential friction factor, $C_{ft1}\,Re^*$, plot the response of $B = 0.2$ is phase-leading as compared with that of $B = 0$ and $B = -0.2$.

Oscillatory effects. Two effects of oscillation, i.e. amplitude and frequency, are addressed in the present section. Figure 9 shows the amplitude effect on the responses of the oscillating thermal-fluid characteristics for $(Re, B, \gamma_0, \omega) = (100, 0.2, -1, \pi)$. As expected the amplitude of the responses strongly depends on the fluctuation of disk rotation. The augmented amplitude of the responses can also result from increasing the amplitude of $\Omega_2(\tau)$.

For the flows of $(Re, B, \gamma_0, \zeta) = (100, 0.2, -1, -0.1)$ and the frequencies $\omega = 0.2\pi$, π, and 2π in Fig. 10, the frequency effects are explored by examining the time-evolution of the friction factors and heat transfer rates in a rotating disk system with the fluctuating disk 2. High-frequency fluctuation leads to a long transient stage before the fully-developed periodicity. Since the fluctuation of the tangential velocity of disk 2 is the source of the disturbance,

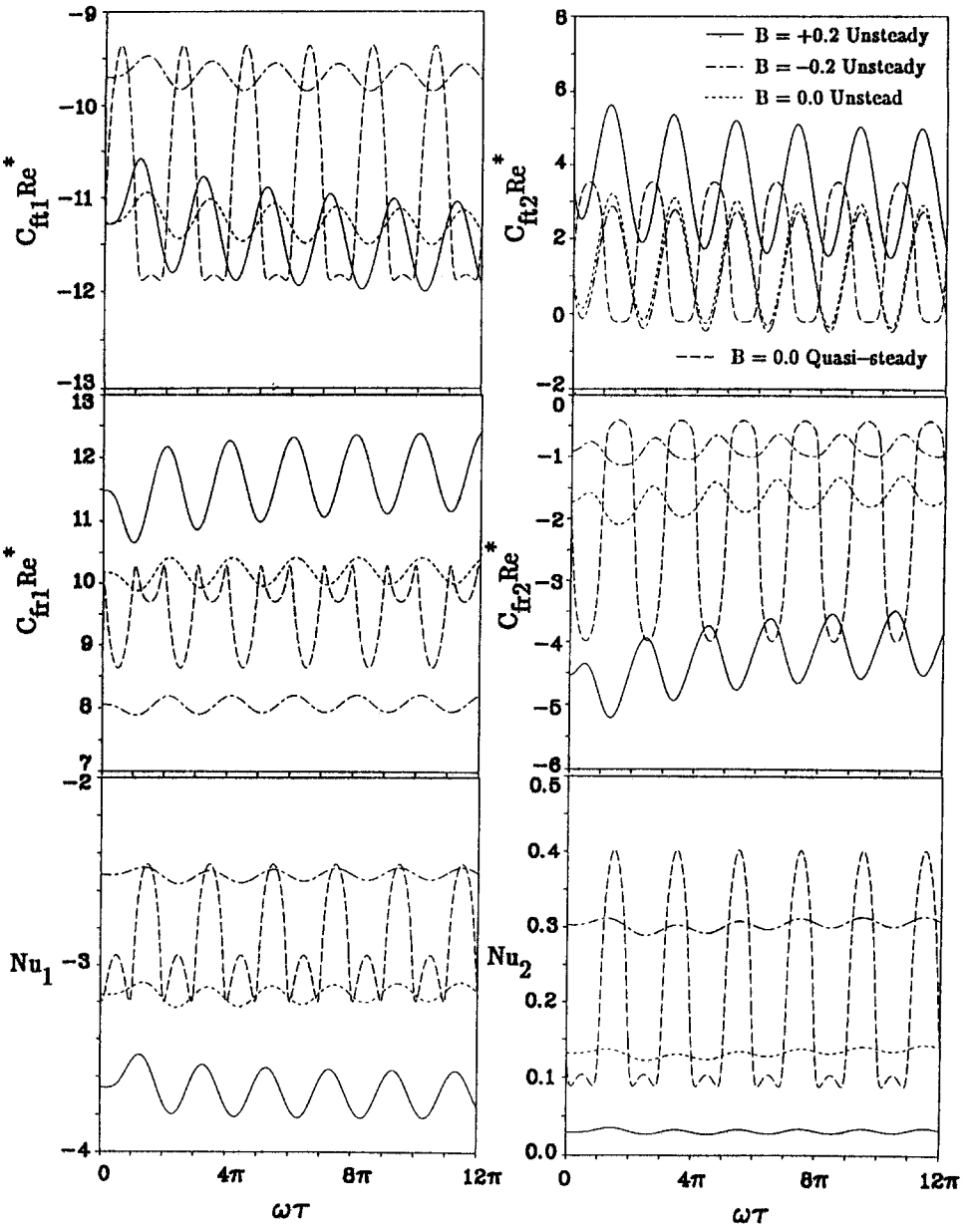

Fig. 8. Centrifugal-buoyancy effects on the flows at $(Re, \gamma_0, \zeta, \omega) = (100, -1, 0.1, 0.2\pi)$.

$C_{ft2}\,Re^{*}$ presents a quite different behavior from the other flow and thermal parameters. It is seen that the amplitudes of the $C_{ft2}\,Re^{*}$ responses can be augmented with increasing fluctuation frequency, and the responses appear phase-leading as compared with the forcing disturbance. For the other parameters, i.e. $C_{ft1}\,Re^{*}$, $C_{fr1}\,Re^{*}$, $C_{fr2}\,Re^{*}$, Nu_1 and Nu_2, the increase in frequency results in a phase lag in responses, and the amplitudes decreased rather than increased. It is believed that they are indirectly influenced by the fluctuation and the fluid cannot respond immediately to the torsional fluctuation of disk 2. Therefore, as presented in Fig. 10, the high frequency of the forcing disturbance leads to the small amplitude of the responses.

Phase diagrams for varying values of Reynolds number. For the condition of $(B, \gamma_0, \zeta, \omega) = (0.1, -1, 0.1, \pi)$ and $Re = 100$, 600 and 1200, the phase diagrams of the velocity functions G vs F at two points adjacent to disks 1 ($\eta \approx 0.08$) and 2 ($\eta \approx 0.91$) are plotted in Fig. 11. The phase diagrams demonstrate the different behaviors of fluid flow near the two disks.

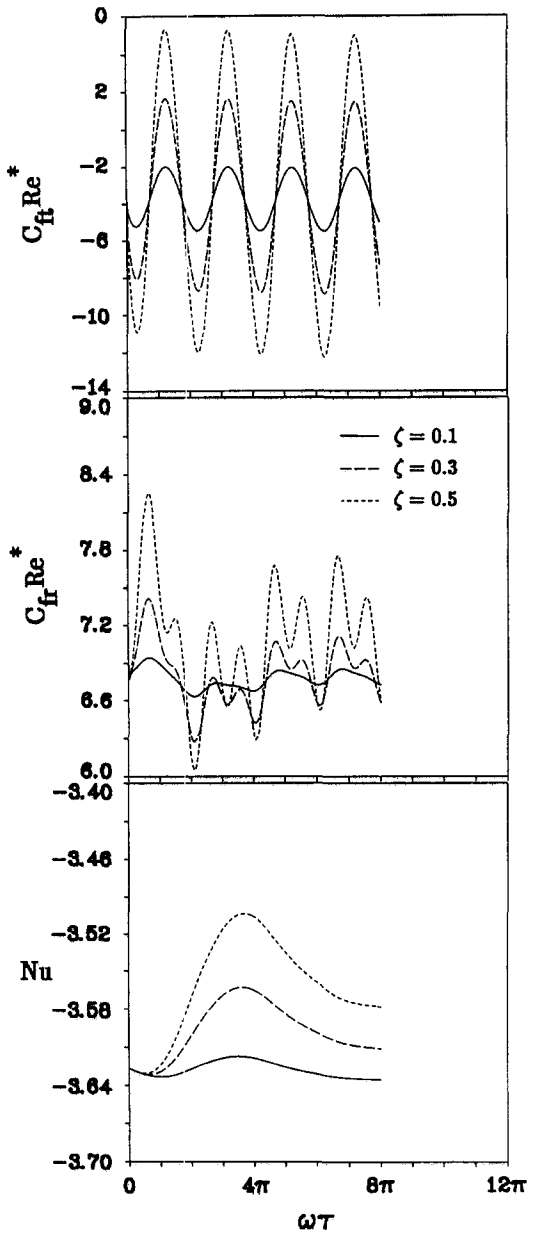

Fig. 9. Amplitudes effects on the flows at (Re, B, γ_0, ω) = (100, 0.2, -1, π).

Near disk 1, from the phase plots in Fig. 11(a), it is observed that the phase trajectories spiral into a small closed path. Physically, it implies that the fluid motion near the constantly-rotating disk (disk 1) decays to an oscillation with a very small amplitude, and the amplitude reduces with increasing Re. The fluid near the fluctuating disk (disk 2) behaves in a more complicated way. As shown in Fig. 11(b), the phase trajectory remains rather regular at a relatively low Reynolds number, $Re = 100$. As the Reynolds number increases to the higher values, e.g. $Re = 600$ and 1200, the phase trajectories first appear anomalous and, eventually, are attracted to a limit cycle in the phase plane. It means that the long-term behavior of the system with $Re \leqslant 1200$ is still a periodic oscillation; but, in the transient stage, the system behaves aperiodically. The phase plots also demonstrate that the increase in Re results in an extension of the transient stage.

CONCLUDING REMARKS

An unsteady analysis for mixed convection between two rotating coaxial disks has been developed. It is believed that the present results are not only useful in exploring the unsteady transport phenomena in a coaxially rotating system, but are also useful in understanding the transient flow and heat transfer characteristics of other unsteady thermal systems. From the present results the following conclusions can be drawn:

(1) For both asymptotic and torsionally oscillatory modes, the flow and heat transfer characteristics experience a transient stage. The system finally reaches a steady state for the asymptotic case, while turning to a fully-developed periodicity in the cases of oscillatory mode. The transient development depends strongly on the competition of the inertia effect of the system and the effects of the unsteadiness.

(2) For the asymptotic mode, centrifugal buoyancy can only alter the steady-state solutions quantitatively; however, the qualitative natures of the transient flow, e.g. the growth and decay of the Ekman layer and the period of the transient stage, cannot be significantly affected by the centrifugal-buoyancy effect.

(3) In the cases of the oscillatory disk, since the torsional oscillation of disk 2 is the source of the disturbance, the tangential friction factor on disk 2 can respond to the forcing oscillation better than the radial friction factors and heat transfer rates; and it is also phase-leading in some of the cases.

(4) The amplitudes of the flow and heat transfer parameters increase with the centrifugal buoyancy in the case of positive thermal Rossby number. The transient stage in the oscillatory mode can be extended by the buoyancy effect. Moreover, the centrifugal buoyancy may cause a phase-shift in the responses.

(5) As expected, the amplitudes of the responses increase with the increasing forcing amplitude. However, the high frequency of the oscillation can augment the amplitude of the tangential friction on the fluctuating disk but suppress the amplitudes of the responses of the other friction factors and heat transfer rates, since the flow can not follow the rapid alternation caused by the high-frequency fluctuation of the oscillatory disk.

(6) For the oscillatory mode, the phase diagram analysis demonstrates that, at high Reynolds numbers, the fully-developed periodicity can be

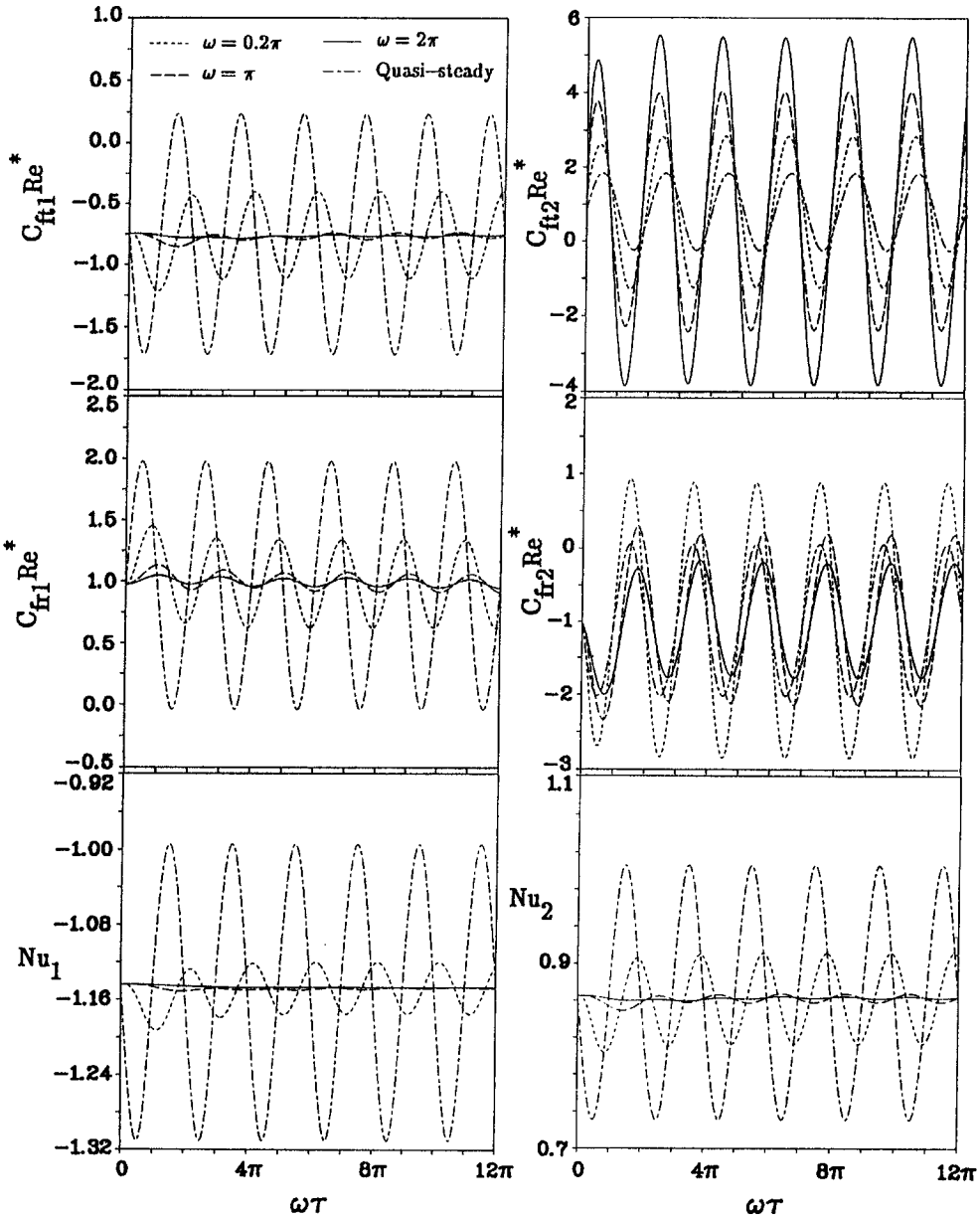

Fig. 10. Frequency effects on the flows at $(Re, B, \gamma_0, \zeta) = (100, 0.2, 0, -0.1)$.

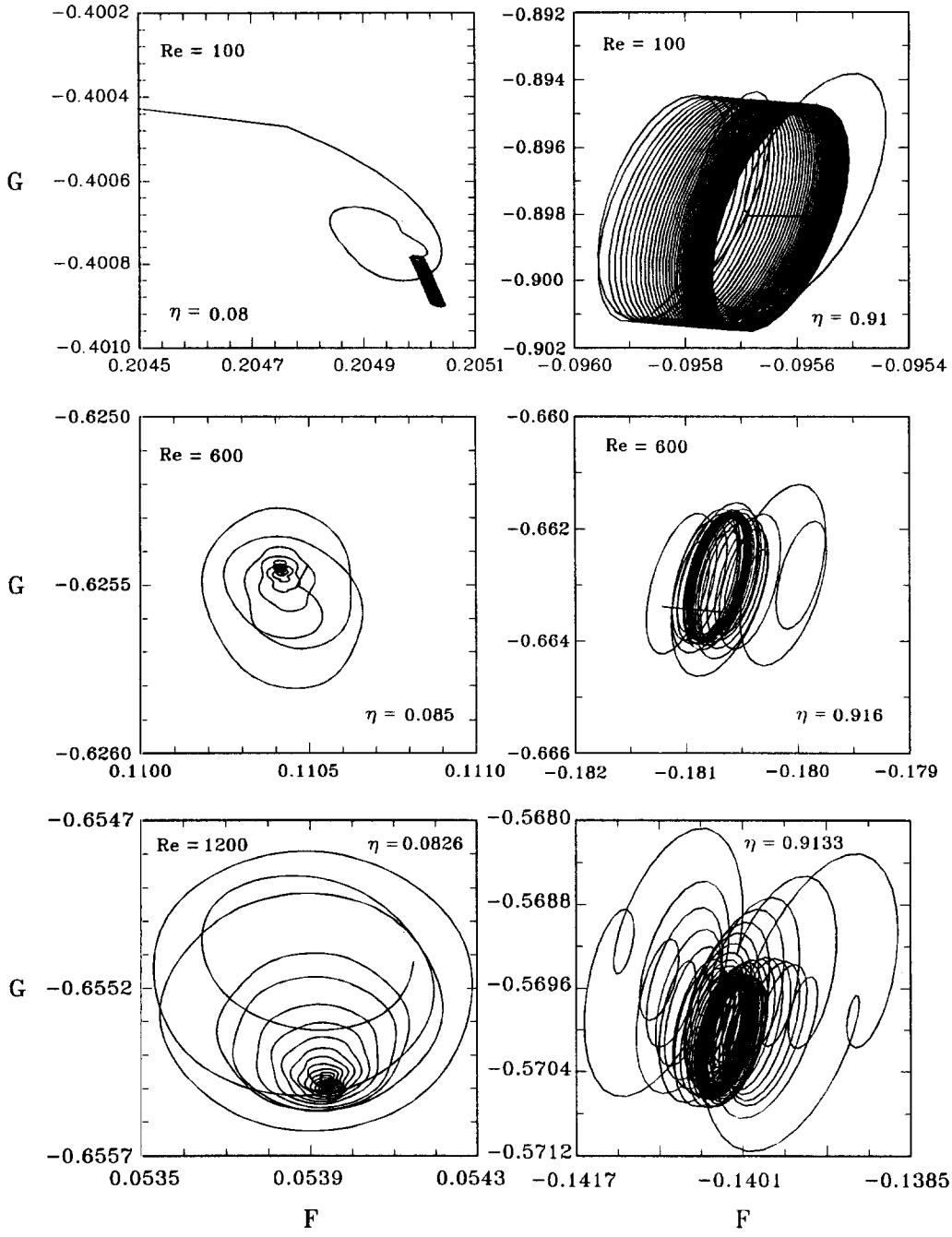

Fig. 11. Phase diagrams of G vs F for $(B, \gamma_0, \zeta, \omega) = (0.1, -1, 0.1, \pi)$ and $Re = 100$, 600 and 1200: (a) flow near disk 1 and (b) flow near disk 2.

delayed and the behavior of the flow system becomes rather anomalous in the transient stage. It may be regarded as a clue to flow approaching instability at the higher Reynolds numbers. The instability problem is beyond the scope of the present work, but it is a worthwhile investigation in the future.

REFERENCES

1. C. Y. Soong, On centrifugal-buoyancy in non-isothermal rotating flows. In *Developments in Theoretical and Applied Mechanics* XVI (Edited by B. Antar *et al.*), II.6.25–II.6.32. UTSI, Nashville, Tennessee (1992).
2. C. Y. Soong and W. M. Yan, Numerical study of mixed convection heat transfer between two co-rotating symmetrically-heated disks, *AIAA J. Thermophys. Heat Transfer* 7(1), 165–170 (1993).
3. C. Y. Soong and W. M. Yan, Transport phenomena in non-isothermal flow between co-rotating asymmetrically-heated disks, *Int. J. Heat Mass Transfer* **37,** 2221–2230 (1994).
4. S. Rosenblat, Torsional oscillations of a plane in a viscous fluid, *J. Fluid Mech.* **6,** 206–220 (1959).
5. D. J. Benny, The flow induced by a disk oscillation in its own plane, *J. Fluid Mech.* **18,** 385–391 (1964).
6. N. Riley, Oscillating viscous flows, *Mathematika* **12,** 161–175 (1965).
7. E. R. Benton, On the flow due to a rotating disk, *J. Fluid Mech.* **24,** 781–800 (1966).
8. N. Riley, Thermally induced boundary-layer flows in a rotating environment, *J. Fluid Mech.* **29,** 241–257 (1967).
9. R. J. Bodonyi and K. Stewartson, The unsteady laminar boundary layer on a rotating disk in a counter-rotating fluid, *J. Fluid Mech.* **79,** 669–688 (1977).
10. R. Purushothaman, Fluctuating flow due to a rotating disk, *Phys. Fluids* **21**(12), 2148–2153 (1978).
11. H. Shippers, Analytical and numerical results for the non-stationary rotating disk flow, *J. Engng Math.* **1**(2), 173–191 (1979).
12. V. P. Sharma, Flow and heat transfer due to small torsional oscillation of a disk about constant mean, *Acta Mechanica* **32,** 19–34 (1979).
13. K. Stewartson, C. J. Simpson and R. J. Bodonyi, The unsteady laminar boundary layer on a rotating disk in a counter-rotating fluid—II, *J. Fluid Mech.* **121,** 507–515 (1982).
14. P. Singh, V. Radhakrishnan, and K. A. Narayan, Fluctuating flow due to unsteady rotation of a disk, *AIAA J.* **27**(2), 150–154 (1989).
15. S. Rosenblat, Flow between torsionally oscillating disks, *J. Fluid Mech.* **6,** 388–399 (1960).
16. C. E. Pearson, Numerical solutions for the time-dependent viscous flow between two rotating coaxial disks, *J. Fluid Mech.* **21**(4), 623–633 (1965).
17. H. P. Greenspan and L. N. Howard, On a time-dependent motion of a rotating fluid, *J. Fluid Mech.* **17,** 385–404 (1963).
18. E. H. Wedemeyer, The unsteady flow within a spinning cylinder, *J. Fluid Mech.* **20**(3), 383–399 (1964).
19. H.-P. Pao, A numerical computation of a confined rotating flow, *ASME J. Appl. Mech.* **37,** 480–487 (1970).
20. H. L. Lugt and H. J. Haussling, Development of flow circulation in a rotating tank, *Acta Mechanica* **18,** 255–272 (1973).
21. M. Bertela and F. Gori, Laminar flow in a cylindrical container with a rotating cover, *ASME J. Fluids Engng* **104,** 31–39 (1982).
22. B. G. Higgins, Film flow on a rotating disk, *Phys. Fluids* **29**(11), 3522–3529 (1986).
23. T. J. Rehg and B. G. Higgins, The effects of inertial and interfacial shear on film flow on a rotating disk, *Phys. Fluids* **31**(6), 1360–1371 (1988).
24. S. Mochiziki, Unsteady flow phenomena and heat transfer in rotating-disk systems. In *Transport Phenomena in Thermal Engineering* (Edited by J. S. Lee, S. H. Chung and K. H. Kim), Vol. 2, pp. 1265–1275. Begell House, New York (1993).
25. M. Itoh, Y. Yamada and K. Nishioka, Experimental study on flow transition due to rotating disk in an enclosure, *J. JSME B* **51/462,** 452–460 (1985) [in Japanese].
26. G. M. Homsy and J. L. Hudson, Heat transfer in a rotating cylinder of fluid heated from above, *Int. J. Heat Mass Transfer* **14,** 1149–1159 (1969).
27. D. D. Gray and A. Giorgini, The validity of the Boussinesq approximation for liquid and gases, *Int. J. Heat Mass Transfer* **19,** 545–551 (1976).
28. J. A. D. Ackroyd, Stress work effects in laminar flat-plate natural convection, *J. Fluid Mech.* **62,** 677–695 (1974).
29. S. L. Lee, A new numerical formulation for parabolic differential equations under the condition of large time steps, *Int. J. Heat Mass Transfer* **26,** 1541–1549 (1988).
30. K. E. Barrett, Numerical study of the flow between rotating coaxial disks, *ZAMP* **26,** 807–816 (1975).
31. C. Y. Soong, An assessment of finite difference methods in solution of singular perturbation problems, Paper presented at the First National Conference on Computational Fluid Dynamics, AASRC, Chito, Taiwan (May 1992).